HHS Public Access

Author manuscript

*Exp Neurol*. Author manuscript; available in PMC 2018 March 01.

Published in final edited form as:

*Exp Neurol*. 2017 March ; 289: 85–95. doi:10.1016/j.expneurol.2016.12.012.

# Adaptive Reorganization of Retinogeniculate Axon Terminals in Dorsal Lateral Geniculate Nucleus Following Experimental Mild Traumatic Brain Injury

**Vishal C. Patel, MD**,

Department of anatomy and neurobiology, Virginia Commonwealth University, Richmond, VA, USA

**Christopher W. D. Jurgens, PhD**,

Department of anatomy and neurobiology, Virginia Commonwealth University, Richmond, VA, USA

**Thomas E. Krahe, PhD**, and

Department of anatomy and neurobiology, Virginia Commonwealth University, Richmond, VA, USA

**John T. Povlishock, PhD [Chairman]**

Department of anatomy and neurobiology, Virginia Commonwealth University, Richmond, VA, USA

## Abstract

The pathologic process in traumatic brain injury marked by delayed axonal loss, known as diffuse axonal injury (DAI), leads to partial deafferentation of neurons downstream of injured axons. This process is linked to persistent visual dysfunction following mild traumatic brain injury (mTBI), however, examination of deafferentation in humans is impossible with current technology. To investigate potential reorganization in the visual system following mTBI, we utilized the central fluid percussion injury (cFPI) mouse model of mTBI. We report that in the optic nerve of adult male C57BL/6J mice, axonal projections of retinal ganglion cells (RGC) to their downstream thalamic target, dorsal lateral geniculate nucleus (dLGN), undergo DAI followed by scattered, widespread axon terminals loss within the dLGN at 4 days post-injury. However, at 10 days post-injury, significant reorganization of RGC axon terminals was found, suggestive of an adaptive neuroplastic response. While these changes persisted at 20 days post-injury, the RGC axon terminal distribution did not recovery fully to sham-injury levels. Our studies also revealed that following DAI, the segregation of axon terminals from ipsilateral and contralateral eye projections remained consistent with normal adult mouse distribution. Lastly, our examination of the shell and core of dLGN suggested that different RGC subpopulations may vary in their susceptibility to

Correspondence to: John T. Povlishock.



The authors do not have any conflicts of interest to report.

injury or in their contribution to reorganization following injury. Collectively, these findings support the premise that subcortical axon terminal reorganization may contribute to recovery following mTBI, and that different neural phenotypes may vary in their contribution to this reorganization despite exposure to the same injury.

**Keywords**

Diffuse Axonal Injury; Traumatic Brain Injury; Lateral Geniculate Bodies; Visual system; Neuronal Plasticity; Axon Terminals

## Introduction

Traumatic brain injury (TBI) is an important public health issue which continues to be a major source of death and disability for healthy adults despite strides in education, prevention, and safety. Mild TBI (mTBI) comprises up to 80% of all TBI cases and many of these patients take up to 6 months to recover from associated disability, with a minority of patients (5–10%) never fully recovering (Bazarian et al., 2005; Cassidy et al., 2004; Corrigan et al., 2010; Dean et al., 2015). Through several studies, the morbidity associated with mTBI has been associated with presence and extent of diffuse axonal injury (DAI) found throughout the subcortical white matter and callosal projections (Christman et al., 1994; Dean et al., 2015; Farkas et al., 2006; Johnson et al., 2013; Kelley et al., 2006; King, 1997; Wolf and Koch, 2016). Of particular note in the pathogenesis of DAI, is that following axonal injury, the axon shaft distal to the injury undergoes degeneration and distal target neurons lose part of their excitatory or inhibitory input. This loss of input is hypothesized to lead to dramatic remodeling in surviving connections, however, literature supporting this premise following TBI is sparse because of the technical challenges associated with following terminal loss and recovery in a diffusely deafferentated network (Büki and Povlishock, 2006; Leunissen et al., 2014; Povlishock and Katz, 2005; Wolf and Koch, 2016).

While multiple brain loci have been linked to the morbidity associated with mTBI, visual circuit dysfunction has been recognized to be a significant contributor to morbidity in the context of mild TBI or concussion (Alvarez et al., 2012; Fimreite et al., 2015; Kapoor et al., 2004; Lachapelle et al., 2008; Lutkenhoff et al., 2013; Schlageter et al., 1993) . Veterans returning from recent foreign conflicts contain a large cohort of patients with visual symptoms due to blast induced TBI (Hoge et al., 2008) . Scalp recordings in post-concussive patients have also demonstrated changes in timing and amplitude of electrical potentials evoked by visual stimulus of increasing complexity as well as decreased luminosity (Fimreite et al., 2015; Papathanasopoulos et al., 2008; Yadav and Ciuffreda, 2013; Yadav et al., 2014) . Collectively, these reports highlight pervasive symptoms in the visual system along with cognitive and memory disturbances associated with mTBI; the latter two of which have previously received significantly more attention (Dymowski et al., 2015; Finnanger et al., 2013).

Because the detailed analysis of DAI and its correlation to morbidity and recovery are impossible to evaluate in humans using current techniques, in the current communication, we move to an animal model of mTBI. To study this question, we exploit the well-

characterized visual axis of the mouse to assess deafferentation and recovery following DAI (Bickford, 2015; Bickford et al., 2010; Guido, 2008; Huberman and Feller, 2008) . Using the mouse central fluid percussion injury (cFPI) model of mild TBI to induce diffuse axonal injury, we have previously reported that the optic nerve reveals a predilection for diffuse axonal injury based on identification of scattered axonal swellings as well as disconnected axonal segments (Wang et al., 2011). Distinct from other modes of optic nerve injury such as cutting, crushing, or stretching, the cFPI model induces only scattered DAI pathology with the sparing of a large fraction of axons, closely approximating the situation found in most cases of concussion and mild TBI (Marklund, 2016; Maxwell et al., 2015; Shultz et al., 2016) . In the experiments described here, we utilize this model to evaluate the downstream changes evoked by injury of the optic nerve and conduct analysis of deafferentation as well as potential reorganization of retinogeniculate axon projections to the dorsal lateral geniculate nucleus (dLGN), a critical structure in the formed vision pathway of mouse.

Through the implementation of anterograde tract tracing of retinal ganglion cells (RGCs) using Alexa fluorescent dyes conjugated to recombinant cholera toxin subunit β (CTB) as well as immunohistochemistry against a well described marker for retinorecipient axon terminals, vesicular glutamate transporter 2 (VGLUT2), we examined deafferentation of dLGN relay neurons through the detection of retinogeniculate axon terminals loss and recovery. Following cFPI induced DAI in the adult mouse optic nerve, we found axon terminal loss occurred in its downstream target, the dorsal lateral geniculate nucleus (dLGN). However, over time, the remaining intact axon fiber population underwent structural reorganization of pre-synaptic terminals in a manner consistent with axon terminal sprouting and adaptive recovery. Our findings support the hypothesis that in the adult mammalian brain, surviving subcortical axons and their axon terminals are capable of dramatic reorganization following mTBI induced DAI. We believe these findings have important implications for our understanding of DAI and its consequences in humans, while providing important insight into the repair and restoration of function following mTBI.

## Materials and Methods

### Experimental Design

Adult male C57BL/6J mice (9–12 weeks) were sourced directly from Jackson Laboratory (Bar Harbor, ME) or bred and maintained in house. Animals obtained directly were kept in house for 48 hours to habituate to our vivarium prior to experiments. Animals were then subjected to mild central fluid percussion injury (1.40 ATM ± 0.05), as previously described (Greer et al., 2013; Hånell et al., 2015; et al., 2013; Wang et al., 2011). In brief, the fluid pressure pulse in this model results in a brief deformation of the brain through an intact dura and induces diffuse traumatic axonal injury in the optic nerve approximately 1mm proximal to the chiasm as well as other neocortical and subcortical sites not addressed in the current study.

As employed, the model involved the induction of general anesthesia in adult male mice with inhaled isoflurane (<5%) before placing their head in a stereotactic frame. Toe pinch reflexes were monitored during surgery and isoflurane concentration adjusted to maintain depth of anesthesia. The skin was opened over the skull and retracted to allow for a 3mm

wide craniotomy midway between lambdoid and bregma cranial sutures. Care was taken to keep the underlying dura intact and a dissecting microscope was used to ensure dural integrity as well as prevention of injury to the large sagittal vascular structures. A luer hub was fixed in place over the craniotomy with dental cement and the animal was allowed to recovery from anesthesia for approximately 1 hour. The animal was then anesthetized (4% isoflurane) again prior to mounting to the fluid percussion device and the impulse delivered to the intact dura of the mouse brain. Sham-injured animals received the same surgeries including, craniotomy, the mounting of the luer hub and attaching the animal to the fluid percussion device, with the absence of the injury that results from release of the pendulum. During surgery to perform craniotomy and implant the luer hub, each mouse was monitored using a pulse oximeter sensor to collect blood oxygen saturation, heart rate, and respiratory rate. Post-injury or sham procedure, return of toe pinch reflex as well as righting reflex were recorded.

The animals were prepared for histologic analysis at 4, 10, and 20 days after injury. The early time point of 4 days was selected to allow axonal disconnection to reach its apogee prior to evaluation of deafferentation based on our previous report (Wang et al., 2011) . We previously examined mTBI retinas for RGC death induced by DAI and demonstrated that the injured/axotomized RGCs continue to survive up to 28 days after injury (Wang et al., 2013) . The time points of 10 and 20 days were chosen based on mouse studies evaluating deafferentation and recovery in the visual axis (Benowitz and Yin, 2008; Lima et al., 2012) . For the histological analyses, the animals were prepared in three difference fashions for either immunohistochemistry, CTB, or routine histopathology. Animals prepared for CTB fluorophore visualization or VGLUT2 immunohistochemistry were sacrificed via intraperitoneal overdose of sodium pentobarbital. Those prepared for CTB visualization were transcardially perfused with 25mL of heparinized 0.9% saline (1u/mL) followed by 200mL of 4% paraformaldehyde dissolved and filtered into Millonig’s buffer (pH 7.4). Animals undergoing VGLUT2 immunohistochemistry or standard histologic preparation in plastic sections were perfused in a similar fashion with the addition of 0.2% glutaraldehyde to the fixative perfusion solution. The brain, optic nerves, and eyes of each animal were post-fixed in their respective fixative for 24 hours and stored at 4 degrees Celsius in Millonig’s buffer until sectioning. All protocols used in this study were approved by the Institutional Animal Care and Use Committee of Virginia Commonwealth University.

## Examination of mTBI induced retinogeniculate axon terminal loss via VGLUT2 immunohistochemistry

For analysis of VGLUT2 immunoreactive axon terminal loss and recovery, animals were prepared as described above for mTBI (1.4 -+0.05 ATM) or sham injury. Sham animals were prepared from littermates of mTBI animals and were sacrificed at similar time points following surgery. Our inclusion criteria were the absence of dural injury during surgical procedures, adequate wound healing following injury or sham-injury, normal feeding and drinking, and normal grooming in days following surgery. All animals prepared for VGLUT2 immunohistochemistry met inclusion criteria and therefore none were excluded from analysis. A total of 6 sham animals together with 4–5 mTBI animals for each post-injury time point were used to generate sections for analysis (Sham N = 6, 4 day mTBI N =

4, 10 day mTBI N = 5, 20 day mTBI N = 5). Free floating coronal sections (40μm) were obtained using a vibrating blade microtome (Leica VT1000 S). We determined a randomized start point and collected alternating sections through the entire left and right dLGN for each animal. Immunohistochemistry was performed on all collected sections by a blinded investigator. Sections were serial washed in phosphate buffered saline (PBS) before incubating for 1 hour at room temperature in blocking solution containing; 0.3M glycine (Sigma-Aldrich), 2.5% bovine serum albumin (Electron Microscopy Sciences), 2.5% normal goat serum (S1000, Vector Labs), in phosphate buffered saline (pH 7.2). Sections were then incubated overnight at room temperature on oscillating stage with 1:2000 dilution of affinity purified rabbit anti-VGLUT2 polyclonal IgG antibody (Synaptic Systems, Cat. No. 135 303) diluted into solution containing; 2.5% BSA, 2.5% NGS, 0.5% triton X-100 (Sigma-Aldrich), in PBS (pH 7.2). Following serial washes in antibody free blocking solution, sections were incubated in poly-clonal goat anti-rabbit IgG antibody conjugated to Alexa 568 (Life Technologies, Cat. No. A-11036) at 1:500 dilution in above blocking solution for 2 hours. Sections were serial washed in PBS, then phosphate buffer, followed by mounting with anti-fade mountant (Life Technologies, Cat. No. P-36931) and cover slipped. Slides were allowed to cure protected from light overnight and edges sealed with nail varnish prior to imaging.

Confocal microscopy was performed for qualitative examination of VGLUT2 positive axon terminals using a Zeiss LSM 700 scanning laser microscope with a Nikon Plan-Apochromat 63×/1.57 objective. The derived Z-stack images were obtained with consideration of Nyquist sampling and saved in CZI format for later examination. Images were processed using Zen Black (Carl Zeiss) to produce maximum intensity projections from Z-stacks.

Quantitative assessment of images obtained from immunohistochemistry for VGLUT2 was performed on sections through dLGN that receive projections from both eyes due to report of potential for reorganization between ipsilateral and contralateral projections following monocular sensory deprivation in adult mice (Coleman et al., 2009; Feldman, 2003). This region is well described as the anterior-posterior (AP) midline of dLGN and can be identified through anatomic landmarks of its borders (Godement et al., 1980). Sections with anatomic or processing artifacts such as large perforating vessels or bubbles in the mountant which could bias analysis were excluded by a blinded investigator. Sections identified in a blinded fashion as containing the anterior-posterior midline of dLGN were imaged using monochromatic mode on a digital camera (Olympus DP 71) mounted to an epifluorescent upright microscope (Nikon E800) and illuminated using LED light source passed through a dichroic filter for 568nm and magnified with a 10× primary objective (Nikon Plan Fluor 10×/0.30). Background fluorescence was removed using background subtraction tool in ImageJ (NIH) with rolling ball radius set to 100. The area surrounding dLGN was cropped out using the polygonal lasso tool in Photoshop CS6 (Adobe) by a blinded investigator and images were converted from greyscale using the threshold function set to 20% such that in the final image, the area around dLGN was white, the area of dLGN was black, and the signal from the immunofluorescent marker was red. Using a custom software module, the number of red pixels were compared to the number of red or black pixels to derive a percent value for the area of each section through dLGN with VGLUT2 immunoreactivity. Sham animals sacrificed and perfused at different time points following surgery were pooled for

analysis. Statistical comparisons between sham and each of the three time points following mTBI were performed as described below in image analysis and statistical methods sections.

## Examination of retinogeniculate axon terminal loss following mTBI through anterograde tract tracing

In a separate experiment, mice subject to sham or mTBI were subjected to intravitreal injection of recombinant cholera toxin subunit β (CTB) conjugated to Alexa 488 or Alexa 594 fluorescent dye (Thermofisher Scientific, Cat. No. C34775 and C34777). This tracer allows visualization of axonal projections and axon terminals without reliance on immunohistochemistry and also allows separation of projections from either eye based on the Alexa dye conjugated to the CTB molecule (Demas et al., 2006; Fort and Jouvet, 1990).

Mice were anesthetized with intraperitoneal injection of Ketamine (10mg/mL) and Xylazine (0.5mg/ml) solution diluted in sterile phosphate buffered saline with delivered volume based on weight of animal (0.01mL/g). A puncture 1mm behind the limbus at the superior temporal aspect of the eye was made using a 30 gauge sterile needle and approximately 3 μl of vitreous fluid aspirated using a pulled borosilicate glass pipet. Using a separate clean pulled glass pipet, 3 μl of 1% CTB reconstituted in sterile phosphate buffered saline was injected using a picospritzer into each eye with CTB conjugated to Alexa 488 injected into the right eye and CTB conjugated to Alexa 594 injected into the left eye for each animal. The pipet was left in place for approximately 30 seconds prior to removal. Body temperature was maintained with a heating pad (Harvard Homeothermic Blanket) during eye injection as well as recovery period before being returned to the vivarium. Animals were sacrificed and perfused with heparinized saline and 4% paraformaldehyde fixative 72 hours following eye injection and post-fixed for 24 hours in 4% paraformaldehyde.

The retinas of all animals were dissected from the remainder of the orbit and flat mounted to glass slides with 0.15 mm thick cover slips superglued in place to either side of the retina before being mounted with Prolong Gold (Life Technologies, Cat. No. P-36931). A larger coverslip was laid to rest on the smaller cover slips to cover the flattened retina and the edges sealed with clear nail varnish prior to imaging on Nikon E800 epifluorescent microscope. A total of 4 animals per mTBI time point or sham cohort were selected for eye injections and projection analysis however animals were rejected and replaced if examination of the retinas post-fixation revealed dural injury, retinal injury, or non-uniform RGC labeling. One animal in the 4 day TBI group was rejected after image acquisition due to high background fluorescence which when subtracted, would also obscure the fluorescent signal such that the result severely under-represented signal from CTB labeled axon terminals. The final number of animals used in analysis is as follows; sham N = 4, 4 day post-mTBI N = 3, 10 day post-mTBI N = 4, 20 day post-mTBI N = 4.

The brains were blocked and free floating coronal sections were obtained at 70μm through the entire length of dLGN on a vibratome and serial mounted to glass slides with Prolong Gold containing DAPI. Slides were allowed to cure protected from light overnight and edges sealed with nail varnish prior to storage at −20 degrees Celsius until imaging. We noted differences in signal to background fluorescence for each of the two fluorophores used as well as between different batches of fluorophores obtained from Thermofisher scientific.

This potential confound was obviated by processing sham and mTBI groups simultaneously and also accounted for by sampling both sides of each brain equally.

For imaging of sections from CTB injected animals, adjustment to exposure time made during imaging due to animal to animal variability in background fluorescence and Alexa signal intensity were kept constant between sections from the same animal. The exposure settings were recorded for each animal and comparable between sham and injury groups. Each fluorophore was imaged using monochromatic mode on the Olympus DP 71 camera attached to a Nikon E800 epifluorescent microscope. Illumination was performed using UV LED light source passed through dichroic filters for Alexa 488 or Alexa 594 depending on the fluorescent channel being captured. Images of all sections through dLGN were examined and all sections through the AP midline for each dLGN were identified by recognition of ipsilateral and contralateral projections by a blinded investigator. Samples were excluded, however, if they contained large anatomic or processing artifacts that obscure the region of interest.

On images of dLGN containing both CTB conjugated Alexa dyes, corresponding to the AP midline of dLGN, the area representing dLGN was cropped out from the surrounding structures using the polygonal lasso tool in Photoshop CS6 (Adobe) by a blinded investigator. The same investigator removed background fluorescence by adjusting the level function in Photoshop for each fluorophore until the fluorescent signal in the adjacent thalamus was no longer present in each sample. Threshold percentage used for conversion of signal images to binary images were also determined by the blinded investigator who used the threshold percent value that best represented the observed signal from the fluorophores (Muir-Robinson et al., 2002; Torborg and Feller, 2004). Threshold percentage ranged from 16% to 63% for both red and green channels with a mean threshold of 30% (+- 7.8% std dev) for the green channel and a mean threshold of 38% (+- 10.0% std dev) for the red channel. The resulting image labeled ipsilateral or contralateral axon terminal projections red or green, the overlap between the two projections as yellow, and the remaining area of dLGN as black. Using again the custom software module, a percentage value was derived for percent of dLGN section area covered by ipsilateral or contralateral projections as well as overlap between ipsilateral and contralateral projections. Statistical comparisons were performed using parametric or non-parametric comparisons between data from sham animals and animals from each time point following mTBI.

### Examination of CTB fluorescent signal within contralateral zone of dLGN

Within the contralateral region of dLGN, which only receives input from the contralateral eye, there are anatomical subgroups of axon terminals that segregate between projecting to the dorsal shell of dLGN and projecting to the inner core (Huberman et al., 2009; Huberman and Feller, 2008; Rivlin-Etzion et al., 2011; Sanes and Masland, 2015). To identify changes within the shell and core, we compared Alexa dye fluorescent signal in images of CTB injected mice after background fluorescence has been removed using the level adjustment tool in Photoshop. Animals prepared for CTB analysis above were re-analyzed through the grey scale images of only contralateral projections in dLGN (Sham N = 4, 4 day mTBI N = 3, 10 day mTBI N = 4, 20 day mTBI N = 4). Using all the sections we collected through the

CTB labeled dLGN, a blinded investigator selected, using ImageJ (NIH), a vertical plot profile through the patch of contralateral projections for each section of dLGN. The optic tract where it enters dLGN was used as the top border while the bottom border was defined by the beginning of the thalamocortical tract in each section (Figure 5A). Sections with anatomic artifact that may bias results were excluded by the investigator. The plot profile values were then normalized to the selected region by subtracting the minimum value from each raw value and dividing the result by the difference between the minimum and maximum fluorescence. The results were then binned at 5% intervals of the depth from surface of the optic tract to derive a final percentage of average fluorescent intensity for each bin (Huberman et al., 2009). Values for each binned width were compared between the three time points and sham animals as seen in Figure 5B.

$$\mathbf{F}\text{value} = (\mathbf{F}\text{raw} - \mathbf{F}\text{min}) / (\mathbf{F}\text{max} - \mathbf{F}\text{min})$$

## Routine histologic screening to assess the presence of DAI in the optic nerve

The eyes and optic nerves of a sham-injured mouse and a 4 day post-mTBI mouse used for immunohistochemistry were dissected free from surrounding structures up to the level of the optic chiasm and removed from the surrounding brain by transection of the optic tract. The orbits of the eyes as well as the associated musculature were removed with sharp dissection from the optic nerves. The remaining optic nerve, chiasm, and beginning optic tract were placed en bloc in 2% osmium tetroxide in 0.1 M phosphate buffer (pH 7.2) for 90 minutes. After serial rinses in 0.1 M Millonig's buffer (pH 7.4), the tissue was then dehydrated with 15 minute incubations in a gradient of cold EtOH dilutions ranging from 30% to 95% in 10% increments. Dilutions stronger than 50% contained 1% uranyl acetate. Finally tissue is dehydrated with 100% EtOH through 3 incubations before incubating with propylene oxide. Tissue is then incubated with propylene oxide and EM resin (Electron Microscopy Sciences) overnight. Next day, tissue is changed into new EM resin for embedding and placed in oven at 55° C. Resin molds containing both the right and left optic nerves were sectioned longitudinally on an ultramicrotome (Carl Zeiss) to produce sections with 1 μm thickness. Sections were then counterstained with toluidine blue before cover slipping with Permount mounting media (Fisher Scientific). Qualitative analysis of optic nerve sections was performed through multiple longitudinal sections to identify DAI pathology as well as intact axons. Images were taken using routine light microscopy with a DP71 digital camera attached to Nikon E800 and 100× oil immersion objective (NA 0.72).

## Image Analysis and Statistical Methods

As reported previously, our injury model induces diffuse axonal injury symmetrically throughout the brain and optic nerves (Greer et al., 2013; Wang et al., 2011). The dLGN on both sides of each animal were treated as internal replicates. Brain sections representing the entire rostrocaudal length of dLGN were identified and all sections through the AP midline of each dLGN were pulled for analysis unless specifically stated otherwise. All sections through the dLGN were treated as independent observations for each group analyzed. Images were analyzed by a blinded investigator to remove background fluorescent signal and/or convert 8-bit images to binary thresholded images. Percentage of dLGN covered by CTB signal or VGLUT2 signal was determined using a custom software module courtesy of

lab of Dr. William Guido. The software used the binary threshold images to compare the number of pixels coinciding with either CTB fluorophores or VGLUT2 fluorescent signal with the number of pixels coinciding with area of dLGN to derive a value for the percentage of dLGN covered by each CTB fluorophore or VGLUT2 fluorescent signal.

Statistical analysis was performed using JMP Pro 11 (SAS Institute Inc.). Determination of whether to use parametric or non-parametric inferential statistics was assessed using Levene's test to compare variance of groups in each dataset. For datasets with equal variance between groups, one-way analysis of variance (ANOVA) was performed, followed by pair-wise comparison utilizing Tukey-Kramer HSD to account for multiple comparisons. For datasets where Levene's test demonstrated unequal distribution of variance, variance was analyzed utilizing the Kruskal-Wallis non-parametric test, followed by Steel-Dwass post-hoc analysis to account for multiple pair-wise comparisons. Statistical significance was set at a $p < 0.05$ for all datasets and all comparisons.

## Results

### Physiological assessment of animals undergoing craniotomy and mild traumatic brain injury

To establish validity of comparison between animal groups, several assessments were made to address potential of experimental variability. Animals weighed prior to surgery showed no significant differences in weight between groups (Sham = 23.23+- 1.55g, 4 day mTBI = 25.82+-0.94g, 10 day mTBI = 24.44 +- 2.82g, 20 day mTBI = 24.54 +- 2.26g; ANOVA $F(3, 30) = 2.024$, $p = 0.132$). Through the use of pulse oximetry during surgery, we found no incidence of hypoxia and no differences with respect to mean arterial blood oxygen saturation (Sham = 96.87 +-2.74%, 4 day mTBI = 96.66+- 1.97%, 10 day mTBI = 96.65+-2.84%, 20 day mTBI = 97.20 +- 1.38%; ANOVA $F(3, 30) = 0.093$, $p = 0.963$) or mean respiratory rate between groups (Sham = 56.34 +-10.11, 4 day mTBI = 65.79 +- 14.96, 10 day mTBI = 59.21 +- 6.58, 20 day mTBI = 60.24 +- 11.67; ANOVA $F(3, 30) = 1.031$, $p = 0.393$). Length of anesthesia used for each animal was also comparable (Sham = 38.92 +- 2.88 min, 4 day mTBI = 39.05 +- 4.40 min, 10 day mTBI = 47.17 +-3.68 min, 20 day mTBI = 43.86 +- 4.11 min; ANOVA $F(3, 30)= 1.06$, $p = 0.380$). Examination of variation in the severity of injury between injury groups as measured in ATM also reveal no differences (4 day mTBI mean = 1.42 +- 0.02 ATM, 10 day mTBI mean = 1.41 +- 0.03, 20 day mTBI mean = 1.42 +- 0.02; ANOVA $F(2, 22) = 0.437$, $p = 0.651$).

Following sham-injury or mTBI, animals were assessed for toe pinch reflex as well as righting reflex, a correlate of the return of consciousness in rodent models. We noted no death, apneic periods, or epileptiform motor movement in any animals following sham-injury or mTBI. While there was no statistical difference in return of toe pinch reflex between groups (Sham mean =37.8+-11.6 sec, 4 day mTBI mean = 33.6+-13.1 sec, 10 day mTBI mean = 60.2 +- 10.9 sec, 20 day mTBI mean = 46.3 +- 12.3 sec; ANOVA $F(3, 30)= 1.03$, $p = 0.394$), with respect to return of righting reflex, we noted a clear delineation between Sham and mTBI animals (Sham mean = 50.0 +- 12.3 sec, 4 day mTBI 244.3 +- 14.0 sec, 10 day mTBI 252.5+- 11.7 sec, 20 day mTBI 257.5 +- 13.1). Due to unequal variance based on Levene's test ($F(3, 30)= 3.089$, $p = 0.042$), nonparametric comparison

using Kruskal-Wallis was performed and found to be significant ($X^2 = 19.945$, $p = 0.0002$). Steel-Dwass post-hoc analysis demonstrated sham righting reflex time was significantly different from each mTBI group (Sham vs 4 day mTBI $p = 0.005$, Sham vs 10 day mTBI $p = 0.002$, Sham vs 20 day mTBI $p = 0.004$).

### Basic pathological response to mTBI: I. Macroscopic change

To confirm the reproducibility of our model, we performed qualitative assessment of brain tissue following sham-injury or mTBI. Consistent with mild TBI, no areas of macroscopic necrosis, contusion, subdural or subarachnoid hemorrhage were found in any of the animals studied. Epidural hematomas were found in both sham and injured animals, however, no volume assessments were performed as the hematomas were always restricted to the craniectomy site and peeled away during removal of the skull or removal of the dural membrane. The underlying brain was always visibly free of hematoma or hemorrhage after dissecting off the meninges.

The optic nerves were intact and non-hemorrhagic, although, at all post-injury time points, bilateral thinning was observed in the optic nerve segments just rostral to the optic chiasm. In contrast, the optic nerves in sham animals maintained a constant thickness along their length. Upon brain sectioning of sham and mTBI animals, no signs of hemorrhage were noted within the ventricles or parenchyma of either group. The mTBI sections did not exhibit any petechial hemorrhages within the cortex, thalamus, or along white matter tracts which is also consistent with the mild nature of our injury model.

### Basic pathological response to diffuse axonal injury: II. Microscopic change

As seen in Figure 1A, plastic embedded thick sections of optic nerve from sham animals demonstrated many thinly myelinated axons as well as their supporting glia and vasculature consistent with previous studies (Inman et al., 2006; Joos et al., 2010; Mabuchi et al., 2003; Mikelberg et al., 1989). At 4 days post-injury, as seen in Figure 1C, microscopy revealed scattered diffuse axonal damage found among numerous intact axons within the optic nerve segments rostral to the chiasm which is consistent with our previous descriptions in this model (Wang et al., 2013, 2011). Examination of VGLUT2 immunoreactivity within dLGN allowed for identification of the retinogeniculate axon terminals downstream of the injured optic nerve. Assessment of this immunoreactivity in our sham-injured animals was consistent with previous reports of normal VGLUT2 immunoreactivity by others (El-Danaf et al., 2015; Hammer et al., 2015, 2014). Within sham animals, the distribution of VGLUT2 immunoreactivity occurred in large clusters of variable size, likely composed of multiple axon terminals as they synapse on proximal dendrites of relay neurons. These axon terminal clusters appeared evenly distributed throughout dLGN, a finding consistent with reports on the normal ultrastructure of retinogeniculate synapses upon relay neurons within dLGN (Bickford et al., 2015, 2010; Guido, 2008; Hammer et al., 2015, 2014; Morgan et al., 2016). Comparison of VGLUT2 immunoreactivity in mTBI animals 4 days post-injury to sham demonstrated the persistence of clusters (Figure 1B & D), however, the clusters in dLGN were more widely separated from each other, suggestive of axon terminal loss.

Further analysis of the optic nerve using CTB conjugated with Alexa fluorescent dyes demonstrated homogeneous filling in sham-injured animals. Coronal cross sections of the optic nerve from the optic disc to the chiasm demonstrated uniform labeling of right and left RGC axon tracts using epifluorescent microscopy (Figure 2B). The right and left RGC axon tracts remained identifiable as they decussated within the optic chiasm into ipsilateral and contralateral fibers for each side of the optic tract. While homogeneous filling was also seen in proximal coronal sections of both optic nerves in mTBI animals, we also noted scattered bright puncta within the injured segment of both optic nerves and drop in fluorescence in sections closer to the chiasm. These findings are correlates of the DAI described above and in previous publications from our lab (Wang et al., 2011). Although not critically evaluated in the current study, it is of note that in both the sham and injured animals the fluorescence was not only homogenously distributed in the optic nerve, but also homogenously distributed in its established downstream projections, including the olivary pretectal nucleus, superior colliculus and LGN.

## Evidence for mTBI/DAI induced deafferentation and reorganization in downstream target dLGN via VGLUT2 immunohistochemistry

To quantify the changes in VGLUT2 immunoreactivity within dLGN of animals at all three time points following mTBI or sham injury, we used an index based on the percentage of the dLGN area occupied by VGLUT2 immunostaining as detailed in the methods section and demonstrated in Figure 3. Specifically, the total area of dLGN that exhibited VGLUT2 immunoreactivity decreased at 4 days post-injury by approximately 26% compared to sham animals (Sham = 61.6%, 4 day mTBI = 45.5%, $p < 0.0001$). However, by 10 days post-injury, we noted a significant increase in area of dLGN demonstrating VGLUT2 immunoreactivity by approximately 22% compared to 4 day post-injury (10 day mTBI = 55.6%, $p = 0.0007$). This increased distribution persisted at 20 days post-injury compared to 4 day post-injury (20 day mTBI = 53.5%, $p = 0.0109$). Of note, neither the 10 day nor the 20 day post-injury group demonstrated full recovery of VGLUT2 immunoreactivity to sham levels and the difference on pairwise comparison was statistically significant for both pairs (10 day mTBI vs sham $p = 0.0493$, 20 day mTBI vs sham $p = 0.0033$). Lastly, pairwise comparison of VGLUT2 immunoreactivity in 10 day and 20 day post-injury groups were found equivalent ($p = 0.816$). Statistical analysis of the derived percentages were examined using Levene's test which demonstrated equal variances in the data from sham and all time points following mTBI ($F(3, 116) = 2.397$, $p = 0.072$). Analysis of variance (ANOVA) between samples from all four groups demonstrated significance of differences in variance ($F(3, 116) = 14.767$, $p < 0.0001$). Pair-wise comparisons between groups were performed utilizing Tukey-Kramer HSD to account for false discovery rate.

## Confirmation of deafferentation and reorganization following DAI using anterograde tract tracing

While VGLUT2 immunohistochemistry in dLGN is specific for retinogeniculate axon terminals in adult mice, it does not allow discrimination of whether the examined axon terminals originated from the ipsilateral or contralateral eye. We therefore performed anterograde tract tracing using fluorescent Alexa dyes conjugated to CTB to label axon terminals in mice that have undergone sham-injury or mTBI at the same time points

addressed using VGLUT2 immunohistochemistry. By injecting recombinant cholera toxin subunit β (CTB) conjugated to Alexa 488 or Alexa 594 into the right or left eye respectively after injury, we identified all retinorecipient brain regions connected to either retina through ipsilateral or contralateral projecting axons. Evaluation of all downstream targets of retinal ganglion cells in sham animals using epifluorescent microscopy demonstrated appropriate labeling of all subcortical targets including the superior colliculus, olivary pretectal nucleus, suprachiasmatic nucleus, ventral LGN, and intergeniculate body in addition to dorsal LGN. Additionally, through the use of the two fluorophores, we observed the distribution of ipsilateral and contralateral projections within these domains as reported by others (Muir-Robinson et al., 2002; Torborg and Feller, 2004). In contrast, the injured animals demonstrated decrease of CTB fluorescent signal in all subcortical targets mentioned above (not shown).

We quantitatively compared retinogeniculate axon terminals between the sham-injury group and the three time points following mTBI as we did using VGLUT2 immunohistochemistry. As noted previously, a percentage value for each section labeled through anterograde CTB labeling was derived as a percentage of dLGN area covered by CTB positive axon terminals from ipsilateral and contralateral projections. The measured overlap was then subtracted from the sum of ipsilateral and contralateral values to derive the percentage of dLGN labeled by axon terminals irrespective of the eye of origin. The derived percentages in each experimental group were then compared and presented in Figure 4. Statistical analysis demonstrated unequal variance between groups using Levene's test ($F(3,97) = 3.927$, $p = 0.0108$). We therefore used Kruskal-Wallis non-parametric comparison to demonstrate significance between groups ($X^2 = 70.945$, $p < 0.0001$). Using Steel-Dwass method to account for multiple pairwise post-hoc comparisons, we noted a 36% reduction in area of dLGN with fluorescent labeling at 4 day post-injury compared to sham-injury ($Z = 6.182$, $p < 0.0001$). Mirroring our findings using VGLUT2 immunohistochemistry, we report that compared to 4 day post-injury, there is 23% increase in fluorescently labeled area at 10 day post-injury ($Z = 3.650$, $p = 0.0015$) and 26% increase at 20 day post-injury ($Z = 4.097$, $p = 0.0002$). Also, as noted for VGLUT2 immunohistochemistry, the partial recovery at 10 and 20 days post-injury did not reach sham values ($Z = 6.223$, $p < 0.0001$ and $Z = 5.980$, $p = < 0.0001$ respectively). Moreover, no statistically significant change was witnessed from 10 day post-injury to 20 day post-injury ($Z = 0.278$, $p = 0.9925$), further suggesting that the axon terminal reorganization demonstrated through both VGLUT2 immunohistochemistry and CTB anterograde tracing did not recovery to sham levels by the time points chosen for this study.

## Evaluation of eye specific axon terminals in dLGN following injury and reorganization in adult mouse

In addition to examination of dLGN area containing retinogeniculate axon terminals, we also examined the deafferentation and the subsequent reorganization response in relation to the overlap of ipsilateral and contralateral axon terminal fields within the AP midline of dLGN. Within this portion of dLGN, ipsilateral and contralateral axon terminals overlap significantly during the perinatal period and strongly segregate before adulthood (Guido, 2008; Huberman et al., 2002). Due to the fact that all retinogeniculate axons express

VGLUT2, our immunohistochemical analysis did not allow direct quantification of axon terminals based on retinal origin. This limitation was overcome by using recombinant CTB conjugated to different fluorescent Alexa dyes for each eye. In adult sham-injured animals, we demonstrated that the retinogeniculate axon terminal population maintained strong segregation of ipsilateral and contralateral inputs to the dLGN with average overlap measured 5.45%. By comparison, when comparing overlap between ipsilateral and contralateral projections in dLGN among TBI animals, there is even less overlap measured between the two axon terminal populations (4 day TBI = 0.68%, 10 day TBI = 1.56%, 20 day TBI = 2.08%) (Figure 4). Statistical analysis of the dataset demonstrated heteroscedasticity of data (Levene's test, $F(3, 97) = 7.672$, $p = 0.0001$) and thus non-parametric comparison using Kruskal-Wallis test was utilized to demonstrate significance between the percent of overlap of ipsilateral and contralateral projections in our comparison groups ($X^2 = 68.4268$, $p < 0.0001$). Each pair-wise comparison of differences using Steel-Dwass post-hoc analysis was found to be significant except for between 10 day vs 20 day post-injury ($Z = 1.8042$, $p = 0.271$). Despite the trend of increasing overlap over time following injury, at 20 days post-injury, the measured overlap was still less than that present in our sham-injury group.

Analysis of only ipsilateral or only contralateral CTB labeled projections demonstrated the same pattern of loss at 4 days post-injury when compared to sham-injury animals, and similar reorganization at 10 days post-injury which persisted at 20 days post-injury. Analysis of variance of ipsilateral projecting retinogeniculate axon terminals demonstrated significance between Sham and TBI groups ($F(3, 97) = 37.80$, $p < 0.0001$). Post-hoc analysis using Tukey-Kramer HSD confirmed significance of difference between Sham and all injury groups, as well as between 4 day post-injury group and both 10 and 20 day post-injury groups ($p < 0.05$). Comparison between 10 day post-injury and 20 day post-injury again demonstrated no significance ($p = 0.91$). Examination of contralateral projections yielded similar results. Due to the differences in variance between groups, non-parametric test was utilized for comparison and demonstrated differences between groups (Kruskal-Wallis, $X^2 = 63.1948$, $p < 0.0001$). Pair-wise comparisons were all found to be significant (Steel-Dwass, $p < 0.007$) except for 10 day post-injury vs 20 day post-injury ($p = 0.999$). These considerations further suggest reorganization within dLGN following mTBI reaches equilibrium prior to reaching the distribution identified in sham animals at the chosen time points used.

## Evaluation of axon terminals from specific RGC subpopulations in the contralateral zone of dLGN following injury and reorganization in adult mouse

In addition to dLGN being divided between regions which receive ipsilateral and contralateral visual input, the contralateral retinorecipient zone in dLGN is further organized into a dorsal shell and ventral core. Both the shell and core of this area in dLGN receive segregated inputs from specific unique subpopulations of retinal ganglion cells that only project to the contralateral dLGN and can be used to further differentiate changes in VGLUT2 immunolabeled as well as CTB labeled axon terminals within dLGN.

In sham animal sections that underwent immunohistochemistry for VGLUT2, there was no significant distinction found in axon terminal distribution between the shell and core of the contralateral zone (Figure 3 – A). By contrast, at 4 days post-injury, we observed a marked drop in VGLUT2 immunolabeled axon terminal clusters in the core of dLGN while the shell appeared relatively spared of axon terminal cluster loss (Figure 3 – B). Moreover, while the distinction between the shell and core persisted at 10 days and 20 days post-injury, the difference in VGLUT2 labeling was less apparent (Figure 3 – C & D). Together, these changes in VGLUT2 expression within the shell and core of the contralateral zone are suggestive of reorganization. Efforts to quantify these differences in the shell and core through VGLUT2 immunohistochemistry were, however, unsuccessful due to narrow dynamic range of fluorescent signal intensity in examined sections.

In contrast to VGLUT2 immunohistochemistry, comparison of the relative fluorescent intensity in dLGN of axon terminals labeled by Alexa fluorophore in CTB injected animals demonstrated relatively stronger fluorescent signal in the shell compared to the core in both sham and mTBI animals (Figure 5B). When we compared the relative fluorescent signal of the shell to the core in sections from 4 day post-injured animals, the difference in relative fluorescence between the shell and core was larger, suggestive of vulnerability of the core to axon terminal loss or general sparing of axons which project preferentially to the dorsal shell. By 10 day post-injury, however, the core demonstrated more fluorescent signal intensity compared to 4 days post-injury and furthermore, at 20 day post-injury, the difference in signal between the shell and core continued to gradually approach the distribution pattern in sham animals. In conjunction with the results of the VGLUT2 immunohistochemistry data analysis, these findings support the premise that following DAI, a reactive response occurs in the intact axon population to repopulate lost input to dLGN relay neurons and that this response maintains eye specific segregation suggestive of adaptive structural plasticity.

## Discussion

In this current study, we utilized the mouse central fluid percussion injury model of mild TBI to induce diffuse axonal injury in the optic nerve. Using with two independent methods to identify the downstream axon terminal fields of injured axons and by evaluating both the deafferentation and reorganization response among axon terminals in dLGN, we provide for the first time, insight into the potential consequences of mTBI induced DAI. One of the three vesicular glutamate transporters expressed in mammalian central nervous system, VGLUT2, is necessary for glutamatergic transmission in the diencephalon where dLGN forms and develops and is the specific isoform of VGLUT present in retinogeniculate axon terminals (El-Danaf et al., 2015; Hammer et al., 2015; Moechars et al., 2006). In this regard, VGLUT2 immunohistochemistry provided us with a highly specific method to identify and compare retinogeniculate axon terminals in dLGN across each time point. As a result, we have exceptional confidence in the quantification of our findings demonstrating axon terminal loss and subsequent reorganization through the analysis of dLGN area with VGLUT2 labeling.

Our use of anterograde axon terminal labeling with CTB conjugated to fluorescent dyes provided further insight into the reorganization of dLGN following DAI. Recombinant CTB labels neurons by irreversibly binding with GM1 gangliosides that diffuse along all fine projections of labeled neurons in both anterograde and retrograde fashion (Fort and Jouvet, 1990). In contrast to immunohistochemistry, anterograde tracing assures that epitope masking or cross reactivity of antibodies is not a confounder, thus increasing sensitivity to find changes in axon terminal distribution. Additionally, by using two different fluorophores conjugated to CTB for right and left eyes in each animal, we were able to demonstrate that not only is there axon terminal loss following DAI and subsequent reorganization, but also that this reorganization maintained the adult pattern of segregation between ipsilateral and contralateral axon terminals within dLGN. Use of an anterograde tracer such as CTB also provided confirmation that the dLGN axon terminals identified in our experiments remained contiguous with their soma of origin as the molecule does not diffuse across synapses or disassociate once it is bound to its target, GM1 ganglioside (Fort and Jouvet, 1990). As CTB diffuses to all projections of labeled neurons, we are again reassured that the observed reorganization is not secondary to changes in strengthened latent connections but rather a structural reorganization among the intact retinogeniculate axon population. While we did not directly examine dLGN for cell loss or subtle structural changes, sections from injured animals did not demonstrate thalamic contusion or intraparenchymal bleeds suggestive of primary dLGN damage that could confound our analysis with either CTB anterograde tracing or VGLUT2 immunohistochemistry. Moreover it is difficult to envision how the large scale adaptive neuroplastic changes observed in this study could occur in a disordered thalamic environment.

In addition to demonstrating the potential for axon terminal reorganization within dLGN of adult mice following mTBI, we have also demonstrated the potential for different subpopulations of retinal ganglion cells to respond differently to DAI. Despite the homogeneous nature of injury within the optic nerve, we observed differences in reorganization between the shell and core of the dLGN contralateral zone. Specifically, axon terminals projecting to contralateral zone shell remained identifiable following injury compared to axon terminals projecting to the contralateral zone core. This finding suggests that RGCs and their axons that project to the shell of dLGN are more resilient than their counterparts projecting to the core. As an alternative hypothesis, the axon terminals within the shell may reorganize more rapidly compared to their counterparts in the core, however, this is less likely. Both possibilities, however, suggest that different RGC subpopulations respond differently to mTBI.

Through the methods employed in this report, we were unable to determine if the RGC subpopulations that innervated the shell and core of dLGN were the same subpopulations that contributed to axon terminal reorganization in those two regions. This issue can be addressed in future investigations using transgenic labeling of retinal subpopulations. Additionally, while we report that retinogeniculate axon terminals reached equilibrium in reorganization prior to 20 days post-injury, we have not determined if this reorganization continues beyond 20 days. The apparent equivalence between our measurements at 10 days and 20 days post-injury may have masked a dynamic process in which axon terminal sprouting occurred concurrently with axon terminal pruning. Further, the lack of functional

or behavioral examination of the visual axis also leaves us without the ability to confirm if the observed reorganization was functionally adaptive or maladaptive. However, as the ventrotemporal retina dominates the contribution to ipsilateral input in dLGN, we believe determination of adaptive vs maladaptive plasticity may be tested through behavioral examination of recovery in central vision or function examination of the binocularly responsive portion of dLGN (Coleman et al., 2009; Howarth et al., 2014; Young et al., 2013). While behavioral or functional examination of plasticity in RGC projections is beyond the scope of our current report, it remains of great importance to further understanding repair and recovery mechanisms following deafferentation within the adult mammalian brain.

Although current literature addressing mTBI demonstrates the occurrence of DAI as assessed via ultrastructure microscopy and histopathologic markers, the implications of deafferentation secondary to axonal injury has yet to be thoroughly addressed. Few have considered that the axon terminal loss associated with DAI, which most likely contributes to the morbidity associated with mTBI, may also set the stage for recovery via axonal plasticity. Other authors have demonstrated axonal plasticity in the rat thalamus and cortex following cFPI, though these studies utilized a higher energy fluid pressure pulse of 1.9 ATM with the goal of modeling moderate TBI while exploring prolonged survival periods (Hall and Lifshitz, 2010; Thomas et al., 2012). Using these models, neuroplastic responses were identified via multiple approaches within both thalamic and neocortical circuits following diffuse injury, albeit that in these studies, the observed neuroplastic responses were recognized to be maladaptive. The reasons underlying the differences between these communications and our findings are at the moment unknown, however, the fact that our experiments evaluated neuroplastic changes within the highly compartmentalized and target specific visual axis may be a factor in these differences. Further, since the studies by Hall and Lifshitz and Thomas et al. evaluated longer time points post-TBI, it is possible that they have unmasked the more chronic sequelae of TBI. These issues merit continued investigation of TBI induced dysfunction and recovery in both sensory pathways.

Comparison of the timing of the observed reorganization in dLGN following injury with literature on synaptic recovery in the hippocampus following cFPI demonstrates a similar temporal framework despite the fact that these studies involved a more severe TBI model (Phillips and Reeves, 2001). The rapid reorganization here shown in dLGN by 10 days following injury is also in line with literature on timing of recovery in connectivity between CA3 and CA1 of the hippocampus by authors who utilized a rat cortical contusion model of TBI (Norris and Scheff, 2009; Scheff et al., 2005). While these reports used different TBI models and did not assess areas involving the visual pathway, together, they demonstrate that neuroplastic reorganization can occur in a similar timeframe in rodent systems following TBI, albeit, in some cases, they may be maladaptive.

Using both VGLUT2 immunohistochemistry and CTB anterograde tracing of retinal ganglion cell axon terminals projecting from the retina to the dLGN, we believe our techniques have the sensitivity and specificity to support the premise that the visual system is capable of adaptive axon plasticity following injury and provides new information on how the mammalian brain responds to mild diffuse axonal injury. In addition to our findings’

general relevance to DAI and potential brain reorganization, we also believe that these studies provide critical insight into the visual symptoms and their course described in those who have sustained mild TBI. Specifically, mTBI patients with visual symptoms that abated or returned to baseline with rehabilitation may be explained by adaptive axon plasticity as presented in this report (Freed and Hellerstein, 1997; Kapoor et al., 2004; Yadav et al., 2014). These human studies support the premise that the structural reorganization we report in the dLGN following mTBI occurs as an adaptive rather than a maladaptive response, however, there is limited information on whether visual dysfunction in humans following TBI is due to DAI in the optic nerve or optic radiations. We hope that based on our findings, the consequences of reorganization in the visual axis and other brain regions vulnerable to DAI will be studied in further detail with renewed attention to axonal plasticity in the remaining intact axons.

## Acknowledgments

This research was supported by the NICHD of the National Institutes of Health under award number R01 HD055813. Microscopy was performed at the VCU Microscopy Facility, supported, in part, by funding from NIH-NCI Cancer Center Support Grant P30 CA016059. The content is solely the responsibility of the authors and does not necessarily represent the official views of the National Institutes of Health.

## Abbreviations

| | |
|---|---|
| **AP** | anterior posterior |
| **cFPI** | Central fluid percussion injury |
| **CTB** | Cholera Toxin β |
| **DAI** | Diffuse axonal injury |
| **dLGN** | Dorsal lateral geniculate nucleus |
| **mTBI** | Mild traumatic brain injury |
| **VGLUT2** | vesicular glutamate transporter 2 |

## Works Cited

Alvarez T, Kim E, Vicci V, Dhar S, Biswal B, Barrett. Concurrent Vision Dysfunctions in Convergence Insufficiency With Traumatic Brain Injury. Optometry & Vision Science. 2012; 89:1740. [PubMed: 23190716]

Bazarian J, McClung J, Shah M, Cheng Y, Flesher W, Kraus J. Mild traumatic brain injury in the United States, 1998--2000. Brain injury. 2005; 19:85–91. [PubMed: 15841752]

Benowitz L, Yin Y. Rewiring the injured CNS: Lessons from the optic nerve. Experimental Neurology. 2008; 209:389–398. [PubMed: 17610877]

Bickford M. Thalamic Circuit Diversity: Modulation of the Driver/Modulator Framework. Frontiers in neural circuits. 2015; 9:86. [PubMed: 26793068]

Bickford M, Slusarczyk A, Dilger E, Krahe T, Kucuk C, Guido W. Synaptic development of the mouse dorsal lateral geniculate nucleus. Journal of Comparative Neurology. 2010; 518:622–635. [PubMed: 20034053]

Bickford M, Zhou N, Krahe T, Govindaiah G, Guido W. Retinal and Tectal “Driver-Like” Inputs Converge in the Shell of the Mouse Dorsal Lateral Geniculate Nucleus. The Journal of

neuroscience: the official journal of the Society for Neuroscience. 2015; 35:10523–10534. [PubMed: 26203147]

Büki A, Povlishock JT. All roads lead to disconnection?--Traumatic axonal injury revisited. Acta Neurochir (Wien). 2006; 148:181–193. discussion 193–4. [PubMed: 16362181]

Cassidy Carroll L, Peloso P, Borg J, Holst H, von Holm L, Kraus J, Coronado V, Injury W. Incidence, risk factors and prevention of mild traumatic brain injury: results of the WHO Collaborating Centre Task Force on Mild Traumatic Brain Injury. Journal of rehabilitation medicine. 2004:28–60.

Christman, Grady, Walker, Holloway, Povlishock. Ultrastructural studies of diffuse axonal injury in humans. Journal of neurotrauma. 1994; 11:173–186. [PubMed: 7523685]

Coleman J, Law K, Bear M. Anatomical origins of ocular dominance in mouse primary visual cortex. Neuroscience. 2009; 161

Corrigan J, Selassie A, Orman J. The Epidemiology of Traumatic Brain Injury. The Journal of Head Trauma Rehabilitation. 2010; 25:72. [PubMed: 20234226]

Dean P, Sato J, Vieira G, McNamara A, Sterr A. Multimodal imaging of mild traumatic brain injury and persistent postconcussion syndrome. Brain Behav. 2015; 5 n/a–n/a.

Demas J, Sagdullaev B, Green E, Jaubert-Miazza L, McCall M, Gregg R, Wong R, Guido W. Failure to Maintain Eye-Specific Segregation in nob, a Mutant with Abnormally Patterned Retinal Activity. Neuron. 2006; 50

Dymowski A, Owens J, Ponsford J, Willmott C. Speed of processing and strategic control of attention after traumatic brain injury. Journal of Clinical and Experimental Neuropsychology. 2015; 37:1–12. [PubMed: 25493696]

El-Danaf R, Krahe T, Dilger E, Bickford M, Fox M, Guido W. Developmental remodeling of relay cells in the dorsal lateral geniculate nucleus in the absence of retinal input. Neural Development. 2015; 10:19. [PubMed: 26174426]

Farkas O, Lifshitz J, Povlishock J. Mechanoporation Induced by Diffuse Traumatic Brain Injury: An Irreversible or Reversible Response to Injury? The Journal of Neuroscience. 2006

Feldman D. Ocular dominance plasticity in mature mice. Neuron. 2003; 38:846–848. [PubMed: 12818169]

Fimreite V, Ciuffreda K, Yadav N. Effect of luminance on the visually-evoked potential in visually-normal individuals and in mTBI/concussion. Brain Injury. 2015; 29:1199–1210.

Finnanger T, Skandsen T, Andersson S, Lydersen S, Vik A, Indredavik M. Differentiated patterns of cognitive impairment 12 months after severe and moderate traumatic brain injury. Brain injury. 2013; 27:1606–1616. [PubMed: 24102501]

Fort P, Jouvet M. Iontophoretic application of unconjugated cholera toxin B subunit (CTb) combined with immunohistochemistry of neurochemical substances: a method for transmitter identification of retrogradely labeled neurons. Brain Research. 1990:209–224.

Freed, Hellerstein. Visual electrodiagnostic findings in mild traumatic brain injury. Brain injury. 1997; 11:25–36. [PubMed: 9012549]

Godement, Saillour, Imbert. The ipsilateral optic pathway to the dorsal lateral geniculate nucleus and superior colliculus in mice with prenatal or postnatal loss of one eye. The Journal of comparative neurology. 1980; 190:611–626. [PubMed: 7400384]

Greer JE, Hånell A, McGinn MJ, Povlishock JT. Mild traumatic brain injury in the mouse induces axotomy primarily within the axon initial segment. Acta Neuropathol. 2013; 126:59–74. [PubMed: 23595276]

Guido W. Refinement of the retinogeniculate pathway. The Journal of Physiology. 2008; 586:4357–4362. [PubMed: 18556365]

Hall, Lifshitz. Diffuse traumatic brain injury initially attenuates and later expands activation of the rat somatosensory whisker circuit concomitant with neuroplastic responses. 2010

Hammer S, Carrillo GL, Govindaiah G, Monavarfeshani A, Bircher JS, Su J, Guido W, Fox MA. Nuclei-specific differences in nerve terminal distribution, morphology, and development in mouse visual thalamus. Neural Dev. 2014; 9:16. [PubMed: 25011644]

Hammer S, Monavarfeshani A, Lemon T, Su J, Fox M. Multiple Retinal Axons Converge onto Relay Cells in the Adult Mouse Thalamus. Cell reports. 2015

Hoge CW, McGurk D, Thomas JL, Cox AL, Engel CC, Castro CA. Mild traumatic brain injury in U.S. Soldiers returning from Iraq. N. Engl. J. Med. 2008; 358:453–463. [PubMed: 18234750]

Howarth M, Walmsley L, Brown T. Binocular Integration in the Mouse Lateral Geniculate Nuclei. Current Biology. 2014; 24:1241–1247. [PubMed: 24856206]

Huberman A, Stellwagen D, Chapman B. Decoupling eye-specific segregation from lamination in the lateral geniculate nucleus. The Journal of neuroscience: the official journal of the Society for Neuroscience. 2002; 22:9419–9429. [PubMed: 12417667]

Huberman A, Wei W, Elstrott J, Stafford B, Feller M, Barres B. Genetic Identification of an On-Off Direction- Selective Retinal Ganglion Cell Subtype Reveals a Layer-Specific Subcortical Map of Posterior Motion. Neuron. 2009; 62:327–334. [PubMed: 19447089]

Huberman, Feller. Mechanisms underlying development of visual maps and receptive fields. 2008

Hånell A, Greer JE, McGinn MJ, Povlishock JT. Traumatic brain injury-induced axonal phenotypes react differently to treatment. Acta Neuropathol. 2015; 129:317–332. [PubMed: 25528329]

Inman D, Sappington R, Horner P, Calkins D. Quantitative correlation of optic nerve pathology with ocular pressure and corneal thickness in the DBA/2 mouse model of glaucoma. Investigative ophthalmology & visual science. 2006; 47:986–996. [PubMed: 16505033]

Johnson V, Stewart W, Smith D. Axonal pathology in traumatic brain injury. Experimental Neurology. 2013; 246:35–43. [PubMed: 22285252]

Joos K, Li C, Sappington R. Morphometric Changes in the Rat Optic Nerve Following Short-term Intermittent Elevations in Intraocular Pressure. Investigative Ophthalmology & Visual Science. 2010; 51:6431–6440. [PubMed: 20688743]

Kapoor N, Ciuffreda KJ, Han Y. Oculomotor rehabilitation in acquired brain injury: a case series. Arch Phys Med Rehabil. 2004; 85:1667–1678. [PubMed: 15468029]

Kelley B, Farkas O, Lifshitz J, Povlishock J. Traumatic axonal injury in the perisomatic domain triggers ultrarapid secondary axotomy and Wallerian degeneration. Experimental Neurology. 2006; 198:350–360. [PubMed: 16448652]

King N. Mild head injury: Neuropathology, sequelae, measurement and recovery. British Journal of Clinical Psychology. 1997; 36:161–184. [PubMed: 9167859]

Lachapelle J, Bolduc-Teasdale J, Ptito A, McKerral M. Deficits in complex visual information processing after mild TBI: electrophysiological markers and vocational outcome prognosis. Brain injury. 2008; 22:265–274. [PubMed: 18297598]

Leunissen I, Coxon J, Caeyenberghs K, Michiels K, Sunaert S, Swinnen S. Subcortical volume analysis in traumatic brain injury: The importance of the fronto-striato-thalamic circuit in task switching. Cortex. 2014; 51:67–81. [PubMed: 24290948]

Lima S, Koriyama Y, Kurimoto T, Oliveira J, Yin Y, Li Y, Gilbert H-Y, Fagiolini M, Martinez A, Benowitz L. Full-length axon regeneration in the adult mouse optic nerve and partial recovery of simple visual behaviors. Proceedings of the National Academy of Sciences. 2012; 109:9149–9154.

Lutkenhoff E, McArthur D, Hua X, Thompson P, Vespa P, Monti M. Thalamic atrophy in antero-medial and dorsal nuclei correlates with six-month outcome after severe brain injury. NeuroImage: Clinical. 2013; 3

Mabuchi F, Aihara M, Mackey M, Lindsey J, Weinreb R. Optic nerve damage in experimental mouse ocular hypertension. Investigative ophthalmology & visual science. 2003; 44:4321–4330. [PubMed: 14507876]

Marklund N. Rodent Models of Traumatic Brain Injury: Methods and Challenges. Methods Mol. Biol. 2016; 1462:29–46.

Maxwell W, Bartlett E, Morgan H. Wallerian Degeneration in the Optic Nerve Stretch-Injury Model of Traumatic Brain Injury: A Stereological Analysis. Journal of Neurotrauma. 2015; 32:780–790. [PubMed: 25333317]

Mikelberg, Drance, Schulzer, Yidegiligne. The normal human optic nerve: axon count and axon diameter distribution. 1989

Moechars D, Weston M, Leo S, Callaerts-Vegh Z, Goris I, Daneels G, Buist Cik, van der Spek Kass S, Meert T, D'Hooge R, Rosenmund C, Hampson M. Vesicular Glutamate Transporter VGLUT2 Expression Levels Control Quantal Size and Neuropathic Pain. The Journal of Neuroscience. 2006; 26:12055–12066. [PubMed: 17108179]

Morgan J, Berger D, Wetzel A, Lichtman J. The Fuzzy Logic of Network Connectivity in Mouse Visual Thalamus. Cell. 2016; 165:192–206. [PubMed: 27015312]

Muir-Robinson G, Hwang B, Feller M. Retinogeniculate axons undergo eye-specific segregation in the absence of eye-specific layers. J Neurosci Official J Soc Neurosci. 2002; 22:5259–5264.

Norris CM, Scheff SW. Recovery of afferent function and synaptic strength in hippocampal CA1 following traumatic brain injury. J. Neurotrauma. 2009; 26:2269–2278.

Papathanasopoulos, Konstantinou, Flaburiari, Bezerianos, Papadakis, Papapetropoulos. Pattern Reversal Visual Evoked Potentials in Minor Head Injury. European Neurology. 2008; 34:268–271.

Phillips LL, Reeves TM. Interactive pathology following traumatic brain injury modifies hippocampal plasticity. Restor. Neurol. Neurosci. 2001; 19:213–235. [PubMed: 12082223]

Povlishock J, Katz D. Update of Neuropathology and Neurological Recovery After Traumatic Brain Injury. The Journal of Head Trauma Rehabilitation. 2005

Rivlin-Etzion M, Zhou K, Wei W, Elstrott J, Nguyen P, Barres B, Huberman A, Feller M. Transgenic Mice Reveal Unexpected Diversity of On-Off Direction-Selective Retinal Ganglion Cell Subtypes and Brain Structures Involved in Motion Processing. The Journal of Neuroscience. 2011; 31:8760–8769. [PubMed: 21677160]

Sanes J, Masland R. The Types of Retinal Ganglion Cells: Current Status and Implications for Neuronal Classification. Annual review of neuroscience. 2015

Scheff SW, Price DA, Hicks RR, Baldwin SA, Robinson S, Brackney C. Synaptogenesis in the hippocampal CA1 field following traumatic brain injury. J. Neurotrauma. 2005; 22:719–732. [PubMed: 16004576]

Schlageter, Gray, Hall, Shaw, Sammet. Incidence and treatment of visual dysfunction in traumatic brain injury. Brain Injury. 1993; 7:439448.

Shultz SR, McDonald SJ, Haar CV, Meconi A, Vink R, Donkelaar P, van Taneja C, Iverson GL, Christie BR. The potential for animal models to provide insight into mild traumatic brain injury: translational challenges and strategies. Neurosci Biobehav Rev. 2016

Thomas T, Hinzman J, Gerhardt G, Lifshitz J. Hypersensitive Glutamate Signaling Correlates with the Development of Late-Onset Behavioral Morbidity in Diffuse Brain-Injured Circuitry. J Neurotraum. 2012; 29:187–200.

Torborg C, Feller M. Unbiased analysis of bulk axonal segregation patterns. Journal of neuroscience methods. 2004; 135:17–26. [PubMed: 15020085]

Wang J, Fox M, Povlishock J. Diffuse traumatic axonal injury in the optic nerve does not elicit retinal ganglion cell loss. Journal of neuropathology and experimental neurology. 2013; 72:768–781. [PubMed: 23860030]

Wang J, Hamm R, Povlishock J. Traumatic axonal injury in the optic nerve: evidence for axonal swelling, disconnection, dieback, and reorganization. Journal of neurotrauma. 2011; 28:1185–1198. [PubMed: 21506725]

Wolf J, Koch P. Disruption of Network Synchrony and Cognitive Dysfunction After Traumatic Brain Injury. Front Syst Neurosci. 2016; 10:43. [PubMed: 27242454]

Yadav N, Ciuffreda K. Optimization of the pattern visual evoked potential (VEP) in the visually-normal and mild traumatic brain injury (mTBI) populations. Brain Injury. 2013; 27:1631–1642. [PubMed: 24111626]

Yadav N, Thiagarajan P, Ciuffreda K. Effect of oculomotor vision rehabilitation on the visual-evoked potential and visual attention in mild traumatic brain injury. Brain Injury. 2014; 28:922–929. [PubMed: 24564831]

Young TR, Bourke M, Zhou X, Oohashi T, Sawatari A, Fässler R, Leamey CA. Ten-m2 is required for the generation of binocular visual circuits. J. Neurosci. 2013; 33:12490–12509. [PubMed: 23884953]

## Highlights

- We confirm that mild traumatic brain injury induces deafferentation in the LGN.
- Diffuse deafferentation in LGN triggers adaptive reorganization among intact axons.
- This reorganization maintains eye specific segregation of axon terminals.
- Different retinal ganglion cell subpopulations may vary their response to injury.

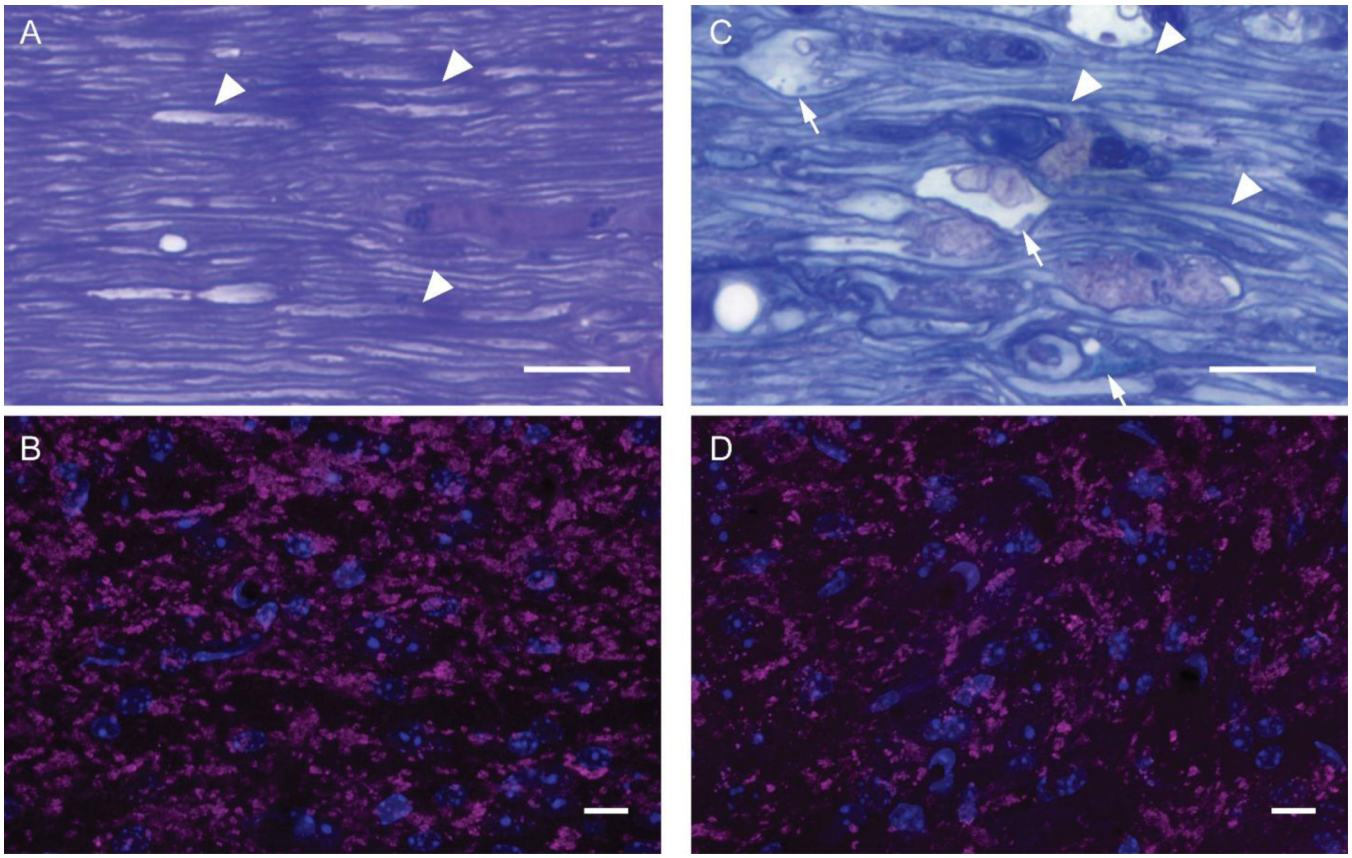


**Figure 1.**

Microscopic evaluation of longitudinal sections through the optic nerves from sham and 4 day post-mTBI mice (A & C) and confocal microscopic evaluation of the downstream axon terminals in dLGN through VGLUT2 immunohistochemistry (B & D). Sham-injured mouse optic nerve revealed normal histology with numerous thinly myelinated axons identifiable (arrowheads). The downstream axon terminals form scattered large clusters visualized in magenta with surrounding cell nuclei visualized in blue (B). By comparision, 4 days after injury, the optic nerve reveals axonal swellings (arrows) with pathologic accumulation of intracellular components and vescicles adjacent to normal appearing thinly myelinated axons (C). Downstream of the injured optic nerve was diffuse reduction in the large clusters of axon terminals visualized in magenta with surrounding nuclei in blue (D). Scale bars = 10 μm.

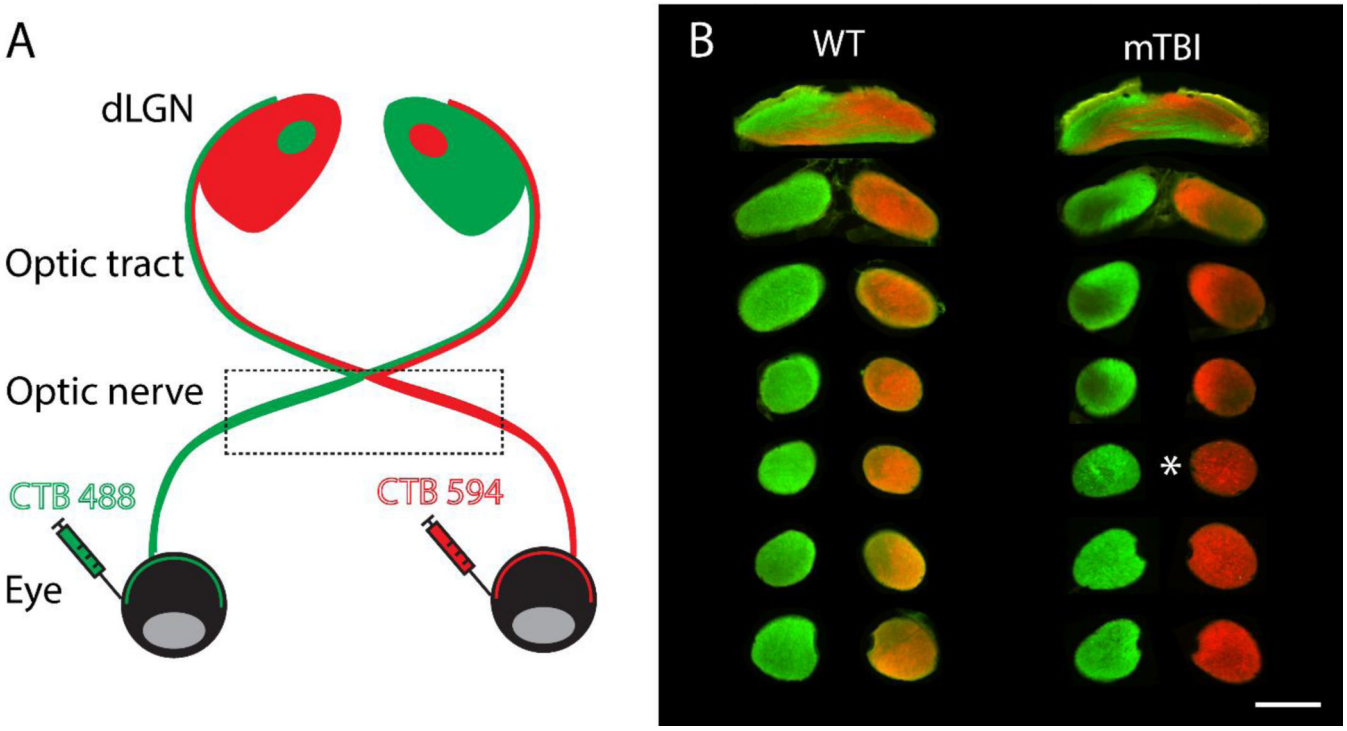


**Figure 2.**

Schematic representation of eye injections and visualization of tracer in the optic nerve. Recombinant cholera toxin β (CTB) conjugated to Alexa fluorescent dyes with two different excitation/emission profiles allow visualization of dLGN projections from the retinal ganglion cells labeled by eye injection of CTB. The projections outlined by the box in panel A are visualized in coronal sections of the optic nerve in panel B from uninjured mouse and 16 day post-injury mouse. Note the loss of fluorescent signal in mTBI sections downstream of the sections with bright puncta (marked with asterisk). Scale bar = 100 μm.

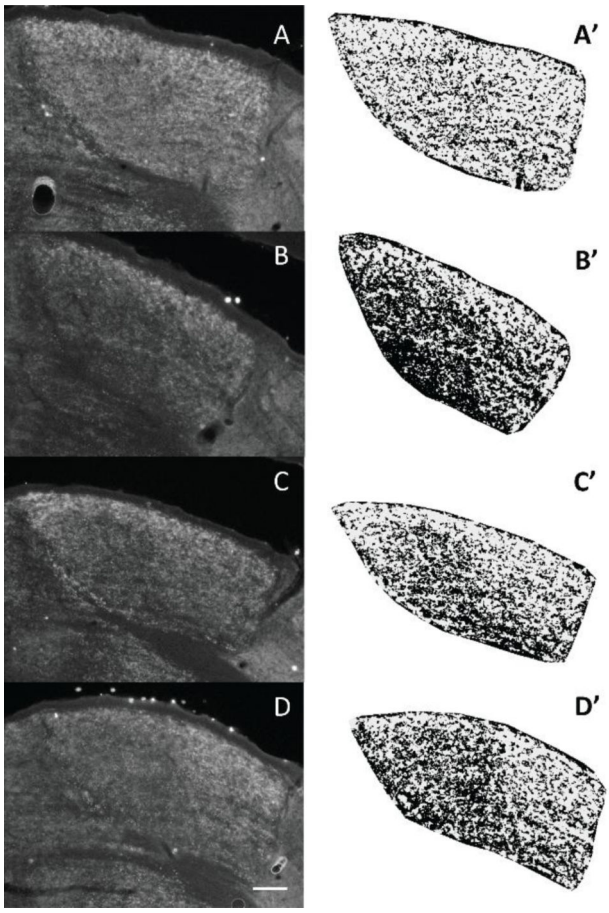


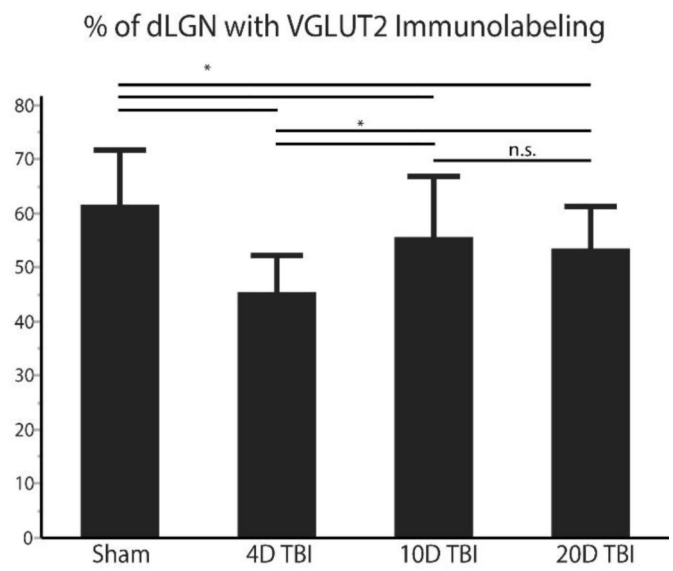


| Level | vs. Level | Difference | Std Err Dif | p-Value |
|---|---|---|---|---|
| Sham | 4D TBI | 16.15150 | 2.451570 | <.0001 |
| 10D TBI | 4D TBI | 10.14314 | 2.547746 | 0.0007 |
| Sham | 20D TBI | 8.11800 | 2.299776 | 0.0033 |
| 20D TBI | 4D TBI | 8.03349 | 2.547746 | 0.0109 |
| Sham | 10D TBI | 6.00835 | 2.299776 | 0.0493 |
| 10D TBI | 20D TBI | 2.10965 | 2.402038 | 0.8161 |

**Figure 3.**

VGLUT2 immunohistochemistry used to identify reorganization in dLGN following mTBI. Representative sections through anterior-posterior midline of dLGN in Sham (A), 4 day post-mTBI (B), 10 day post-mTBI (C ), 20 day post-mTBI (D) are shown in grey scale prior to cropping surrounding image and conversion to binary image using threshold of 20% of illuminescence (A' – D'); scale bar is 100μm. Data from each section is pooled by experimental group and the means compared using ANOVA with post-hoc pairwise comparison using Tukey-Kramer correction with p-values as shown in the table below graph. (Sham n = 36, 4D TBI n = 24, 10D TBI n = 30, 20D TBI n = 30; astrisk represents p-value < 0.05 for comparisons).

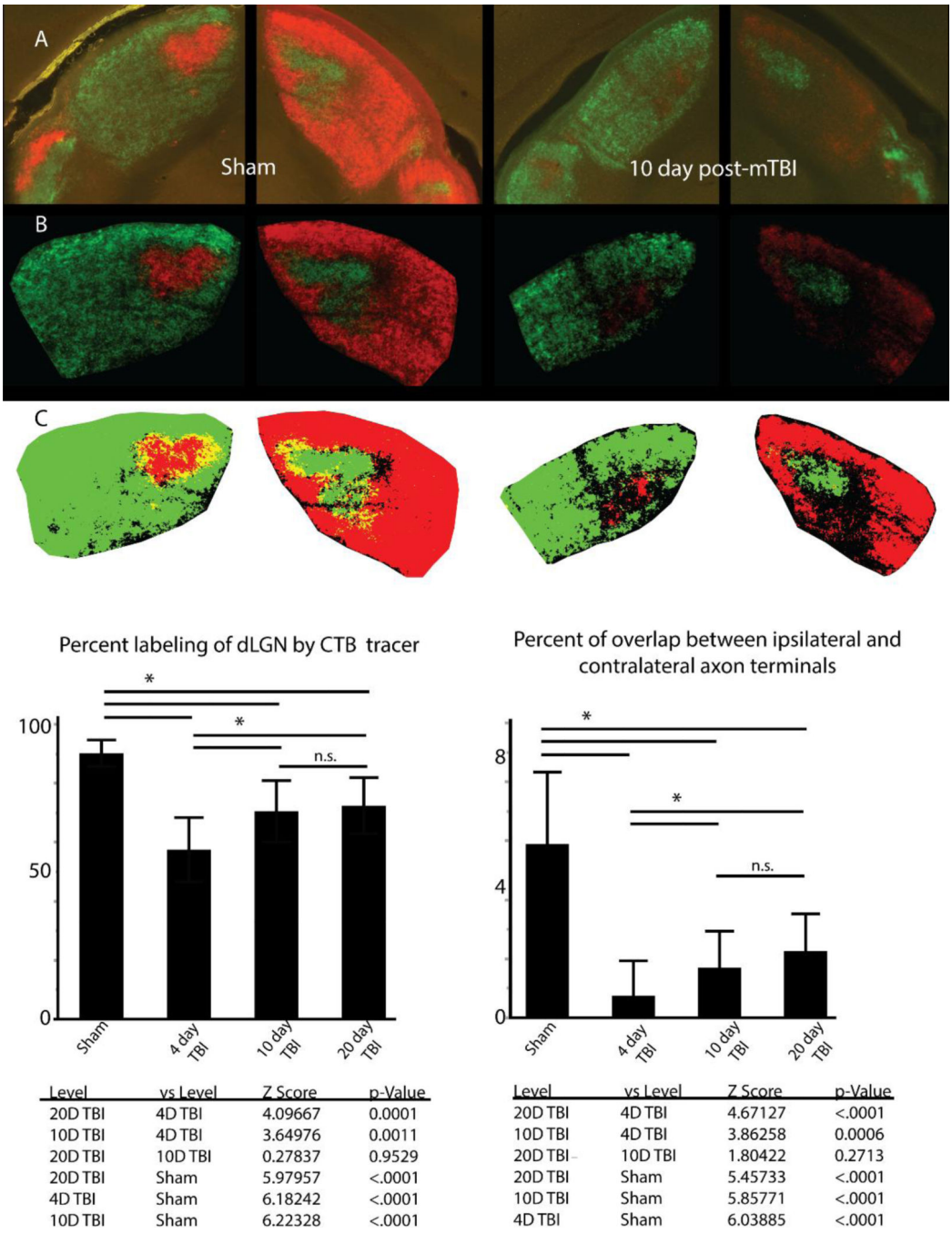


| Level | vs Level | Z Score | p-Value |
|---|---|---|---|
| 20D TBI | 4D TBI | 4.09667 | 0.0001 |
| 10D TBI | 4D TBI | 3.64976 | 0.0011 |
| 20D TBI | 10D TBI | 0.27837 | 0.9529 |
| 20D TBI | Sham | 5.97957 | <.0001 |
| 4D TBI | Sham | 6.18242 | <.0001 |
| 10D TBI | Sham | 6.22328 | <.0001 |

| Level | vs Level | Z Score | p-Value |
|---|---|---|---|
| 20D TBI | 4D TBI | 4.67127 | <.0001 |
| 10D TBI | 4D TBI | 3.86258 | 0.0006 |
| 20D TBI | 10D TBI | 1.80422 | 0.2713 |
| 20D TBI | Sham | 5.45733 | <.0001 |
| 10D TBI | Sham | 5.85771 | <.0001 |
| 4D TBI | Sham | 6.03885 | <.0001 |

**Figure 4.**

Through the use of CTB conjugated to Alexa dyes to label retinogeniculate axon terminals, we find uniform labeling of ipsilateral and contralateral projecting axon terminals within both sides of dLGN (A). Images are adjusted for background fluorescence (B) before conversion to binary color scale images (C) for quantification of axon terminal reorganization. Examination of the percent of dLGN labeled by both ipsilateral and contralateral projecting axon terminals demonstrates a significant loss at 4 days post-injury which recovers at 10 days and 20 days post-injury. Examination of overlap between

ipsilateral and contralateral projections demonstrates reorganization involves changes in the overlap between the two fiber populations however segregation is maintained relative to sham condition. Error bars derived from standard deviation. Asterisk over bars indicate comparison p value is < 0.05, n.s. = no significance.

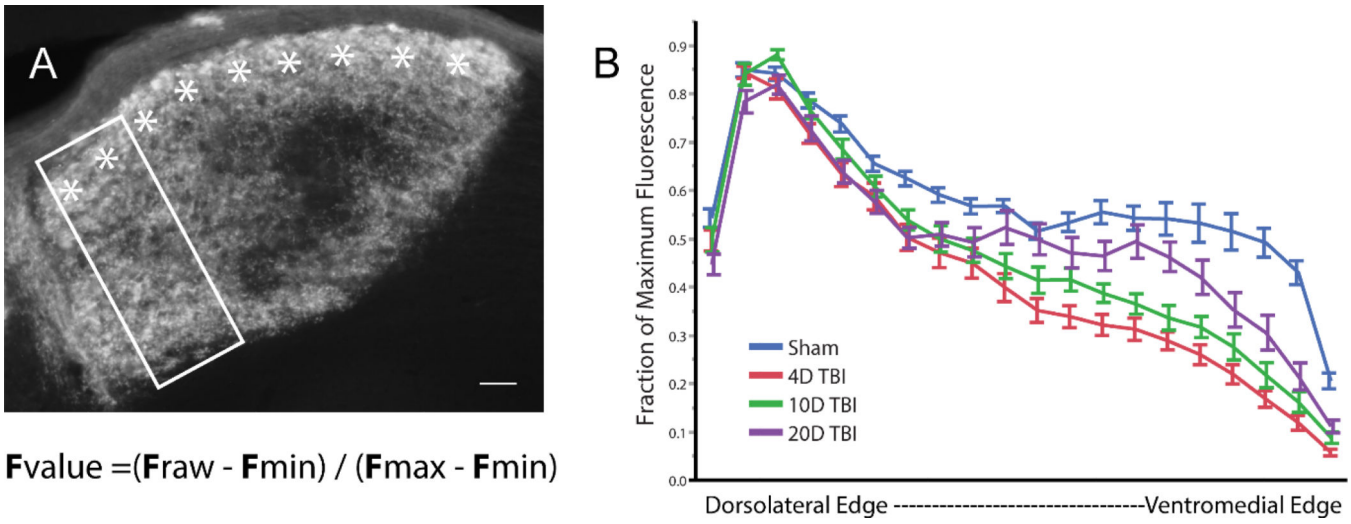


**Figure 5.**

In panel A, a section of dLGN from a sham mouse injected with CTB is shown. The shell is marked with asterisks. Using a rectangular window, we measured the plot profile of Alexa dye pixel intensity along the depth of the dLGN within the region receiving only contralateral inputs using methods described by Huberman et al. We normalized the values at each position along the depth using the formula above, where Fmin is the minimum fluorescence value, Fmax is the maximum fluorescence value, and Fraw is the signal intensity along each pixel width of the box for each given section. Normalized fluorescence values were binned at 5% intervals of the depth and averaged across all sections from all animals in each experimental group. Panel B demonstrates the change in fraction of max fluorescence as one moves from the dorsolateral edge to the ventromedial edge of dLGN for each group. Scale bar = 20um. Bars represent SEM. N = 3 to 4 animals per group with 3 to 4 samples per dLGN per animal.